Supporting Information

Synthesis of Ferromagnetic Cobalt Nanoparticle Tipped CdSe@CdS Nanorods: Critical Role of Pt-activation

Lawrence J. Hill,[a] Nathaniel E. Richey,[a] Younghun Sung,[b] Philip T. Dirlam,[a] Jared J. Griebel,[a] In-Bo Shim,[c] Nicola Pinna,[d*] Marc-Georg Willinger,[e] Walter Vogel,[f] Kookheon Char,[b*] and Jeffrey Pyun[a,b*]

[a]Department of Chemistry and Biochemistry, University of Arizona, 1306 E. University Blvd., Tucson, AZ 85721, USA , [b]World Class University Program for Chemical Convergence for Energy and Environment, The National Creative Research Initiative Center for Intelligent Hybrids, School of Chemical and Biological Engineering, Seoul National University, Seoul 151-744, Korea, [c]Department of Nano and Electronic Physics, Kookmin University, Seoul, 136-702, Korea, Fax: 82-2-910-5170 ; Tel:82-2-910- 4757, [d] Institut für Chemie, Humboldt-Universität zu Berlin, Brook-Taylor-Straße 2, 12489 Berlin, Germany, [e] Department of Inorganic Chemistry, Fritz Haber Institute of the Max Planck Society, [f] Department of Chemistry, National Central University, Taiwan.

Email: jpyun@email.arizona.edu, nicola.pinna@hu-berlin.de, khchar@snu.ac.kr.

SUPPORTING INFORMATION

1. Materials and methods: 1,2,4-trichlorobenzene (TCB) (> 99%) was purchased from both Aldrich and Alfa Aesar and passed through a 0.2 micron syringe filter prior to use. 1,2-dichlorobenzene (DCB) (> 99%) was purchased from both Aldrich and Acros Organics and passed through a 0.2 micron syringe filter prior to use. 1,2-hexadecanediol (HDD) (90%), toluene (99.5%), cadmium(II) oxide (CdO) (99.5%), selenium (99.999%), oleic acid (OLAC) (90%), oleylamine (OLAM) (70%), and 1-octadecene (ODE) (90%) were purchased from Aldrich. Octadecylphosphonic acid (ODPA) (97%), trioctylphosphine oxide (TOPO) (99%), trioctylphosphine (TOP) (90%), trioctylphosphine (TOP) (97%), hexylphosphonic acid (HPA) (97%) and dicobalt octacarbonyl stabilized with 5% hexanes ($Co_2(CO)_8$) were purchased from Strem. Platinum (II) acetylacetonate ($Pt(acac)_2$) (98%) and diphenyl ether (DPE) (99%) were purchased from Acros Organics. Sulfur (>99.0%) was purchased from EMD, and absolute ethanol (EtOH) was purchased from Pharmco-Aaper. All chemicals were commercially available and used as received, unless otherwise noted. Air-free manipulations were performed under argon by using standard Schlenk techniques with vacuum pressure at approximately 1 mm Hg using an Edwards High Vacuum International vacuum pump (Model RV12, Sussex England). An Omega temperature controller CSC32K with a K-type utility thermocouple and a Glas-Col fabric heating mantle were used for thermolysis reactions. All centrifugation steps were performed in 50 mL centrifuge tubes using a rotor with a radius of 11 cm. UV-vis measurements were obtained using a Shimadzu Corporation UV-vis recording spectrophotometer (no. UV-2401PC, Kyoto Japan). CdSe quantum dot diameters were estimated from UV-vis data by using the correlation of quantum dot diameter with the low energy visible absorbance maximum reported by Peng et al.[1] Fluorescence measurements were obtained using a Photon Technology International spectrometer (no. 3005, Weatherford TX). Low resolution bright field TEM images (those not labeled "high resolution") were obtained on a Phillips CM12 transmission electron microscope (CM12) at 80 kV, or a Tecnai Spirit transmission electron microscope (FEI) at 100 kV using in house prepared carbon coated copper grids (Cu, hexagon, 200 mesh). Image analysis was performed using ImageJ software (Rasband, W.S., National Institutes of Health, http://rsb.info.nih.gov/ij/, 1997-2007) from bright field TEM images at a minimum of 110000x magnification by sizing a minimum of 100 particles (unless otherwise stated). Relative uncertainty of particle size determinations using ImageJ was found to be 1 % of diameter average (e.g., 20 ± 0.2 nm). High resolution TEM

(HRTEM) and high-angle annular dark field scanning transmission electron microscopy (HAADF-STEM) images were acquired using a CM200FEG (Philips) microscope with a field emission gun operated at 200 kV or a Cs corrected FEI Titan operated at 300 kV. Thermogravimetric analysis was carried out under nitrogen atmosphere using a TGA Q50 instrument and software from TA Instruments. XRD measurements were performed on the μSpot beam line at BESSY II synchrotron.[2] A Si 111 Monochromator was used and an incident X-ray energy of 12.48 keV (0.9933 Å) was selected. The beam size was 100 μm. A polymer sample holder with 2 mm holes and a thickness of about 1 mm was used. Samples were filled into the holes and covered with Scotch tape. To protect the area detector (MAR-CCD) the primary beam was blocked by a 3.5 mm beam stop made of lead. Each sample was measured twice with an acquisition time of 150 s. The program Fit2D was used for integration of the images.

2. Synthesis of Pt-activated nanorods and CoNP-tipped nanorods

CdSe quantum dots and CdSe@CdS nanorods.
CdSe quantum dots and CdSe@CdS nanorods were synthesized as previously reported,[3] which was modified from the methods of Manna et al.[4]

Synthesis of Pt-activated CdSe@CdS nanorods.
CdSe@CdS nanorods were activated to promote matchstick Co-deposition based on kinetic observations of the Pt-deposition reaction previously reported by us,[3] using a modification of the Pt-deposition conditions of Mokari et al.[5] CdSe@CdS nanorods (CdSe seed: D = 3.2 nm; nanorod: L = 66.0 nm, D = 5.3 nm, 43 mg, 20 wt-% organic content by TGA, approximately 8 nanomol nanorods) were weighed into a 20 mL vial and dispersed in 1,2-dichlorobenzene (1.2 mL) *via* vortex agitation, where sonication in certain cases was briefly applied (< 2 minutes). A solution of platinum(II) acetylacetonate (1 mg in 0.1 mL DCB; 2.5 μmol) was then transferred to the vial containing the nanorod dispersion *via* syringe no more than 5 minutes prior to use (see below).

Phenyl ether is a low melting solid, and was heated to 40 °C in a water bath prior to use. Diphenyl ether (10 mL at 40 °C), oleic acid (0.2 mL; 0.61 mmol), oleylamine (0.2 mL; 0.63 mmol), and 1,2-hexadecanediol (43 mg; 0.17 mmol) were weighed into a 50 mL three-neck-round bottom flask equipped with a reflux condenser and 1" magnetic stir bar. The flask was fitted with rubber septa and a temperature probe was passed through a septum until it came into direct contact with the solution. The solution was then heated to 80 °C *in vacuo* for 30 minutes using a heating mantle and temperature controller with continuous stirring at 300 RPM and subsequently backfilled with Ar. The contents of the flask were then heated to 225 °C under argon, followed by injection *via* syringe of CdSe@CdS nanorods dispersed in a solution of $Pt(acac)_2$/DCB (described above) to the reaction mixture. The heating mantle was removed from the reaction flask after 30 seconds from the injection of $Pt(acac)_2$/nanorods/DCB. Toluene (10 mL) was injected *via* syringe into reaction mixture once the internal temperature of the medium reached 100 °C, and the orange dispersion was allowed to cool to room temperature prior to purification.

Purification of as synthesized Pt-activated nanorods in this toluene dispersion was accomplished *via* 3 cycles of dissolution, precipitation, and centrifugation. The room temperature, crude, product (i.e., toluene dispersion) was transferred to a 50 mL centrifuge and diluted with toluene (to 30 mL) before adding EtOH (15 mL) to induce precipitation. Centrifugation of this heterogeneous mixture (3500 RPM, 12 min) afforded an orange pellet. The clear supernatant was decanted and the pellet was dispersed in toluene (30 mL) before diluting with EtOH (15 mL). Centrifugation (3500 RPM, 12 min) a second time afforded an orange pellet. The yellow-tinted, translucent, supernatant was decanted and the pellet was dispersed in toluene (30 mL) before diluting with EtOH (15 mL). Centrifugation (3500 RPM, 12 min) a third time resulted in an orange pellet. The yellow-tinted, translucent, supernatant was decanted and the resulting precipitate was dispersed in DCM (approximately 10 mL total) before a sample was taken for TEM in toluene (DCM dispersion (0.2 mL) diluted into toluene (3 mL) in a separate vial). The DCM dispersion was transferred to a tared vial *via* glass pipet and the solvent was evaporated before drying the sample *in vacuo* at 55 °C overnight to yield an orange powder (32 mg, 20.6 wt-% organic content from TGA).

The extent of nanorod activation was sensitive to small changes in reaction time and concentration of $Pt(acac)_2$. The optimal ratio of $Pt(acac)_2$: CdSe@CdS nanorods was found to be 1 mg (2.54 μmol) $Pt(acac)_2$: 8 nmol CdSe@CdS nanorods. Higher $Pt(acac)_2$: nanorod ratios and longer reaction times afforded more activated nanorods with an increased tendency towards deposition of CoNP-tips onto both nanorod termini and lateral facets. The effects of the very short Pt-activation step on CdSe@CdS nanorods were difficult to visualize by bright field TEM imaging (Fig. 1b). Nanorod dimensions were also observed to be unaffected by this short Pt-activation step. Furthermore, XRD (Fig. 4) of CdSe@CdS

nanorods subjected to this short Pt-activation step was essentially unchanged relative to the initial wurtzite structure of unmodified CdSe@CdS nanorods which was in agreement with previous reports utilizing more harsh Pt-deposition conditions.[3, 5] Optical spectroscopy was also found to be comparable before and after Pt-activation, where fluorescence quenching of nanorod emission was not observed after Pt-activation (Fig. S-8 and S-9).

General considerations for Co-deposition (procedures follow under the next bold heading)
Deposition of large, dipolar, CoNP-tips onto Pt-activated CdSe@CdS nanorods was carried out by dispersing Pt-activated nanorods in a solution of polymer ligand (PS-COOH) in high boiling solvent (TCB), followed by heating the concentrated dispersion to the target temperature before injecting a solution of the cobalt precursor ($Co_2(CO)_8$). $Co_2(CO)_8$ / TCB solutions were prepared at least 20 minutes prior to use and subjected to vigorous vortex agitation to promote complete dissolution of the cobalt precursor. *Care should be taken during injection of $Co_2(CO)_8$/TCB due to the large amount of carbon monoxide which is evolved during injection which, aside from being a poisonous gas, can splash the reaction mixture onto the sidewalls of the glassware and increase the likelihood of obtaining polymodal products.* Product morphology was sensitive to dilution of the reaction mixture (Fig. S-4). The morphology of the CoNP-tipped products was strongly dependent on the temperature used during the Co-deposition step, with 160 °C being the optimized temperature. Maintaining a precise temperature during the short reaction times used here was challenging in practice, and reaction temperatures in the range of 155-160 °C were deemed optimal since higher temperatures tended to result in more free CoNPs and CoNP inclusions per nanorod (Fig. S-6). In short: higher quality CoNP-tipped products were obtained by holding the reaction temperature at or below 160 °C during the Co-deposition reaction. The use of an end-functional polymer ligand was advantageous during cobalt-deposition since the larger size of these ligands imparted additional steric stabilization of strongly associating dipolar CoNP-tips in comparison to small molecule ligands.

Synthesis of dipolar matchstick CoNP-tipped CdSe@CdS nanorods.
Matchstick dipolar CoNP-tipped nanorods were prepared using our established conditions to grow ferromagnetic CoNPs.[6-8] Carboxylic acid-terminated polystyrene (PS-COOH) was synthesized by ATRP as previously reported and used for all Co-deposition reactions (M_n = 8600 g/mol by GPC versus polystyrene; PDI = 1.07).[7]

A stock solution of $Co_2(CO)_8$ (300 mg, 0.9 mmol) dissolved in TCB (3 mL) was prepared in a glass vial before setting up the Co-deposition reaction. The vial was sealed with a screw top cap and left to stand under ambient conditions (20 minutes) before vigorous vortex agitation (no sonication) for several minutes to promote complete dissolution of all solids. The vial was then subjected to vortex agitation for an additional 2 minutes.

Pt-activated CdSe@CdS nanorods (5 mg for 66.0 nm nanorods with 20.6% organic content by mass, approximately 0.95 nanomol) were loaded into a 20 mL vial containing PS-COOH (10 mg; 1.2 μmol), and TCB (1 mL) was added before the vial was fitted with a screw top polypropylene cap and subjected to 10 minutes sonication. A 10 mm magnetic stir bar was added to the vial after sonication, and the vial was fitted with a rubber septum. A temperature probe was passed through the septum until it came into direct contact with the reaction mixture before securing the septum with electrical tape. The reaction vessel was evacuated for 2 minutes and backfilled with argon before heating to 160 °C using a heating mantle and temperature controller with continuous stirring (1000 RPM). Upon reaching 160 °C, room temperature $Co_2(CO)_8$ dissolved in TCB (0.5 mL of the $Co_2(CO)_8$ stock solution described above; approximately 50 mg or 146 μmol of $Co_2(CO)_8$) was injected. The temperature was held at 160 °C for 15 minutes from the time of injection before the vial was removed from the heating mantle and allowed to cool to room temperature.

The crude reaction mixture at this stage contained the target matchstick dipolar CoNP-tipped nanorods along with a fraction of both unmodified nanorods and CoNP-tipped nanorods with smaller, non-dipolar CoNP inclusions. The proportion of dipolar, CoNP-tipped nanorods was enriched by collecting the dipolar nanorods *via* magnetic isolation methods onto a custom built magnetic probe (see Fig. S-2 and S-3). A solution of PS-COOH in TCB (2 mg PS-COOH : 1 mL TCB) was used for all washing steps to prevent excess stripping of polymer ligands from the sample. In the first step of this magnetic purification process, removal and rinsing of the magnetic stir bar was required using a solution of PS-COOH/TCB (3 mL) to recover the magnetically associated crude product. The recovered mixture was then diluted with DCM (to approximately 12 mL) before being shaken by hand and subjected to vortex agitation (sonication of these materials resulted in nanorod fracture), after which the magnetic probe shown in Fig. S-2 was immersed into the dispersion to promote magnetic flocculation of dipolar nanorods onto the exterior of the magnetized assembly. After immersion of the probe into this DCM dispersion for 2 minutes, a black precipitate was observed to accumulate along the length of the probe (Fig. S-3 inset). The protective sleeve (syringe barrel) was detached from the metal cylinder and bar magnet accessory, and the viscous black ink was washed from the sleeve exterior into another vial using PS-COOH/TCB

(3 mL). The black dispersion was then diluted to 12 mL with DCM before collecting onto the magnetic probe as above. The entire process was repeated for a total of 3 magnetic collection steps per sample. The pellet obtained from the final magnetic collection step was dispersed in PS-COOH/TCB (3 mL) and a sample was cast directly from this dispersion onto a carbon coated copper grid for TEM imaging (no DCM was added to the final product). The product was imaged *via* TEM and sized using ImageJ software (CoNP-tip diameter = 20 ± 4 nm; approximately 88% of dipolar CoNPs imaged carried a nanorod side chain). These CoNP-tipped matchsticks were sensitive to sonication which resulted in an increased number of shorter "broken" free nanorods being observed in sonicated samples.

Dipolar CoNP-tipped nanorods were stored as dispersions in PS-COOH/TCB when intended for further use, since drying of these heterostructures was observed to result in irreversible flocculation of these samples. The dispersion of CoNP-tipped nanorods in PS-COOH/TCB was precipitated and dried strictly to enable yield determination (described below). The final TCB dispersion was transferred to a centrifuge tube *via* pipet and diluted to 20 mL with MeOH prior to centrifugation at 10000 RPM for 5 minutes, which yielded a black pellet. The clear supernatant was decanted and PS-COOH (20 mg, 2.4 µmol) was added before dispersing the pellet in DCM (3 mL) to ensure sufficient material remained after drying for characterization by TGA. The DCM dispersion was transferred to a tared vial *via* glass pipet and the solvent was evaporated before drying the sample *in vacuo* at 55 °C overnight to yield a black powder (43 mg, 66.6 weight-% organic content from TGA). The final yield of inorganic material was calculated to be 14 mg.

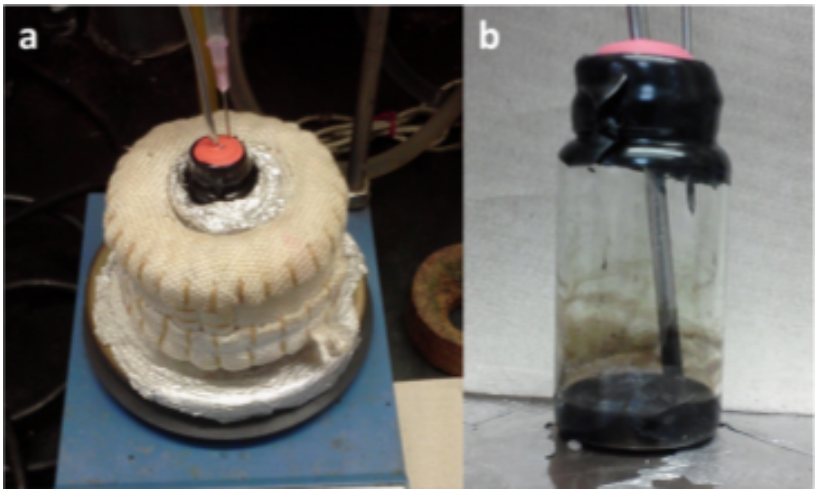

Figure S-1: Small scale Co-deposition reaction setup, as discussed in the procedure for Co-deposition onto CdSe@CdS nanorods (CdSe seed: D = 2.7 nm; nanorod L = 69.1 nm; D = 6.0 nm). Small scale Co-deposition reactions (50 mg $Co_2(CO)_8$, scaled for 0.96 nmol Pt-activated nanorods) were carried out in 20 mL scintillation vials using a heating mantle, 10 mm stir bar, and temperature probe (a). An image of the crude reaction mixture (15 minutes after injection of $Co_2(CO)_8$) is shown in panel S-1-b.

Cobalt deposition reactions for the products shown in this work were carried out in 20 mL glass scintillation vials (as described in the Co-deposition procedure and shown in Fig. S-1). These small reaction scales afforded economical use of material, and purification was greatly simplified by use of a custom built magnetic probe shown in Fig. S-2. This magnetic collection method quickly yielded well-dispersed products which were largely free of unreacted nanorods. A magnetic probe was used to allow selective magnetic isolation of the CoNP-tipped nanorods due to the ferromagnetic nature of the material. Glass vials (20 mL) were used (as opposed to wider glassware such as beakers) to promote close contact of the probe with the entire dispersion during the collection step. In addition, it was useful to be able to remove the magnetic interactions prior to rinsing the magnetic fraction from the probe, and the protective sleeve was useful for this purpose, as shown in Fig. S-2-and S-3. Lastly, a solution containing the stabilizing ligand used in the nanoparticle synthesis (PS-COOH in TCB, 2 mg / mL) was used for all rinsing steps to retain colloidal stability and avoid stripping excess ligands during rinsing steps (Fig. S-3 and Co-deposition procedure).

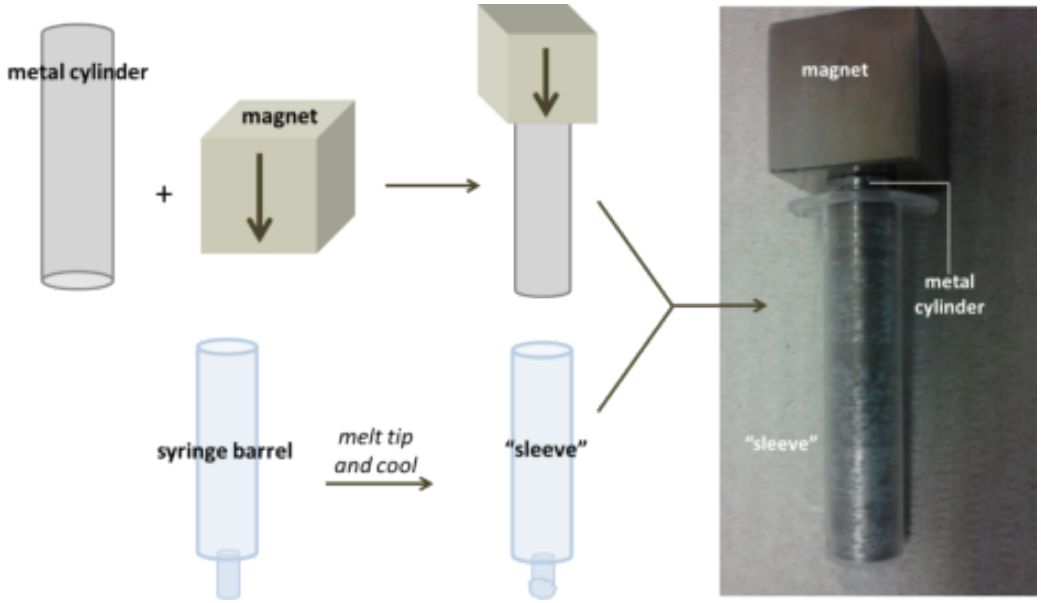

Figure S-2: Custom built magnetic probe used for purification of CoNP-tipped matchsticks. The assembly consisted of three parts: syringe barrel, metal cylinder, and magnet. The small end of a plastic 5 mL syringe barrel (Norm-Ject) was sealed to create a protective sleeve by heating the tip of the syringe until it melted using a hot surface, and cooling to room temperature (bottom). A cylinder of ferrous metal (rolled steel) was machined so that it fit snugly into the barrel of the syringe (cylinder dimensions: L = 64 mm, D = 12 mm) while being just long enough to attach to a strong magnet (Nickel-coated NdFeB, grade N52; Surface Field: 6,451 Gauss; Brmax: 14,800 Gauss; dimensions: 1" x 1" x 1") to complete the assembly (top). The sleeve was fitted over the metal cylinder before use, and the image to the right shows the completed assembly referred to as a "magnetic probe". Note: the syringe barrel used here served only as a protective sleeve, which prevented the metallic portions of the magnetic probe from coming into direct physical contact with liquid dispersions during purification (shown below in Fig. S-3). Since the syringe tip was melt-sealed, the interior volume of the syringe barrel was inaccessible.

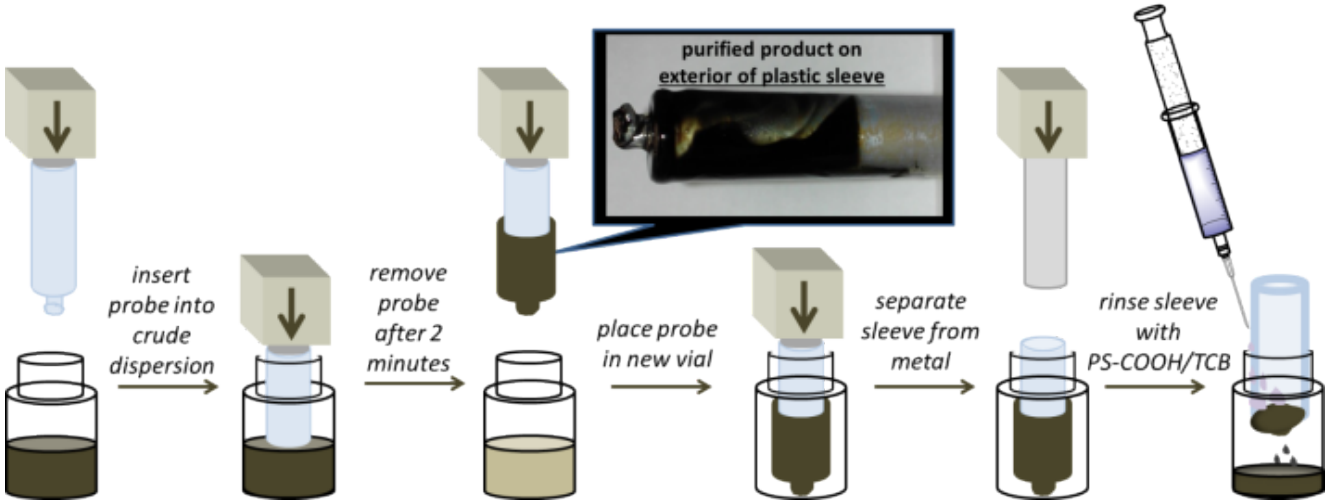

Figure S-3: Scheme for purification of dipolar CoNP-tipped nanorods by magnetic collection, as described in the procedure for Co-deposition. The magnetic probe described in Fig. S-2 was lowered into a dispersion containing both CoNP-tipped nanorods and free nanorods and left to stand for two minutes. Magnetic association of the metal cylinder with dipolar particles in the dispersion occurred through the thin barrier imposed by the plastic sleeve, which prevented direct physical contact of the metal cylinder with the NP dispersion. The probe was then removed and black material enriched in dipolar product was present along the exterior of the protective sleeve, as shown in the inset. The probe was then placed into a new vial and the metallic portion was separated from the sleeve. The dipolar product was then rinsed into this vial, in the absence of magnetic interactions, using a solution of PS-COOH in TCB as described in the procedure for Co-deposition. The purified sample was diluted further and the entire process was then repeated for a total of 3 cycles.

3. Control experiments for nanoparticle synthesis

Control experiment: Co-deposition using twice the amount of TCB solvent

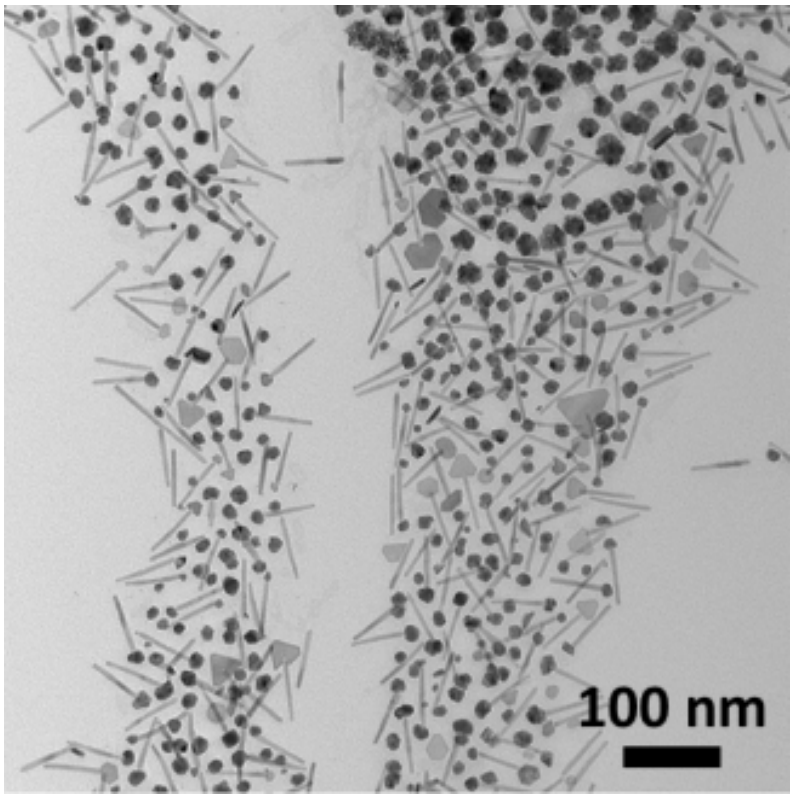

Figure S-4: Diluting the entire cobalt deposition reaction mixture twofold (by using twice the amount of TCB relative to the standard conditions) resulted in the appearance of free CoNPs in addition to CoNP-tipped nanorods.

Mixtures of CoNP-tipped heterostructures and free CoNPs were observed in products obtained by diluting the Co-deposition reaction mixture twofold (by using twice the volume of TCB solvent). An apparent increase in the number of nanorods with laterally attached CoNPs was also observed, which might point to contribution from an etching mechanism under more dilute conditions similar to that observed by Cozzoli et al.[9] Interestingly, the increased activation of these nanorods relative to unmodified CdSe@CdS nanorods was able to compete with homogeneous nucleation of free CoNPs for consumption of Co monomers even under these more dilute conditions (Fig. S-4).

Smaller CoNP-tips were observed after decreasing only the concentration of $Co_2(CO)_8$, though many of these CoNP-tips appeared to be fused together in the crude product. Product morphology was not sensitive to moderate variations (approximately a factor of 2) in the concentration of PS-COOH used during Co-deposition other than a decrease in colloidal stability with decreasing ligand concentration. Using 1,2-dichlorobenzene (DCB) in place of TCB gave similar results, though DCB correlated with the observation of more free CoNPs – possibly due to faster precipitation of Co.

Control experiments: the role of $Pt(acac)_2$ concentration during activation as observed in the CoNP-tipped products.

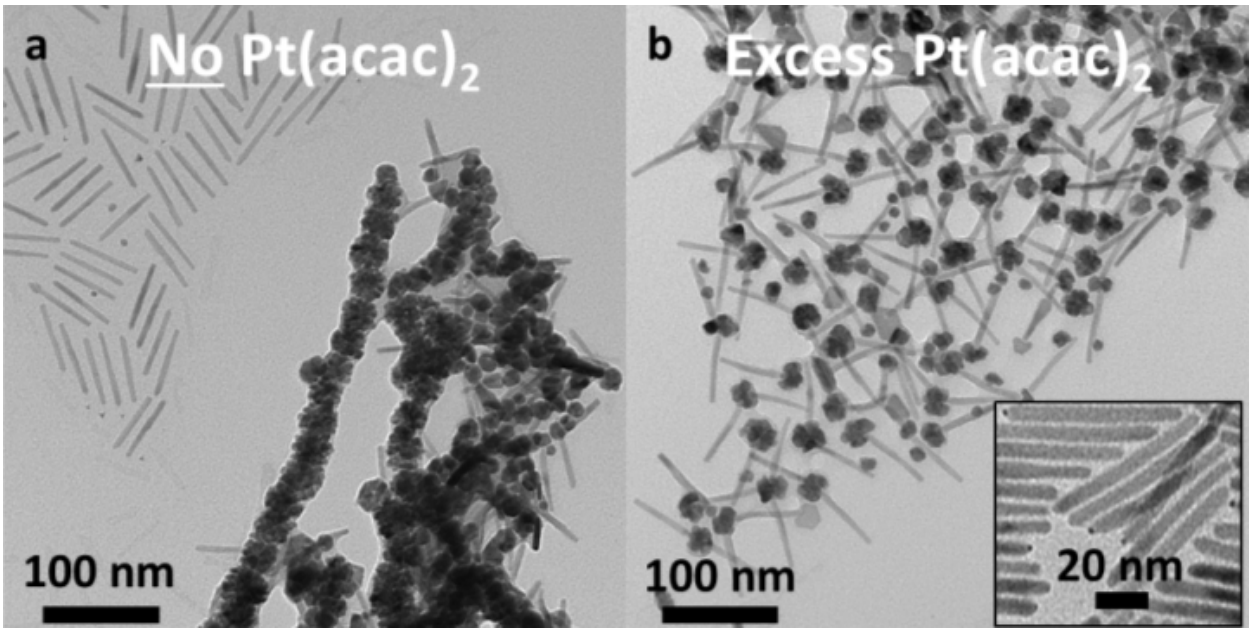

Figure S-5: TEM images of samples cast directly from the crude reaction mixture after cobalt deposition onto nanorods activated without using $Pt(acac)_2$ (a), and with excess $Pt(acac)_2$ at 5x the concentration in the standard procedure (b). The inset in panel b shows the PtNP-tipped nanorods obtained from activation with a fivefold excess of $Pt(acac)_2$.

We investigated the role of $Pt(acac)_2$ in the activation of CdSe@CdS nanorods. As previously reported,[3] the other reagents present during this activation step can alter the reactivity of these nanorods towards Co-deposition. The experiments shown in Fig. S-5 examined cobalt deposition onto nanorods activated without $Pt(acac)_2$ (Fig. S-5a), and with five times the concentration of $Pt(acac)_2$ under conditions otherwise identical to the optimized conditions (Fig. S-5b).

Removing $Pt(acac)_2$ from the activation conditions (given in the representative procedure for the synthesis of dipolar CoNP-tipped nanorods) resulted in fewer nanorods receiving a CoNP-tip after Co-deposition, and free CoNPs and free nanorods were observed to be the major product (Fig. S-5a). By comparison, activating nanorods with a fivefold excess of $Pt(acac)_2$ relative to the representative procedure resulted in PtNP-tips which were observable by standard bright field TEM imaging (Fig. S-5b-inset). However, Co-deposition onto these PtNP-tipped nanorods resulted in heterostructures more commonly having CoNPs attached at lateral facets and on both termini (Fig. S-5b), and these CoNP-tips were commonly smaller than the dipolar CoNP-tips obtained from nanorods activated under the optimized conditions. Taken with the other control experiments included here, the apparent number of CoNP/nanorod increased with the amount of $Pt(acac)_2$ used during activation and with activation time (manuscript Fig. 1, Fig. S-5). CoNP-tips are assigned to the sulfur-rich nanorod facet of these Pt-activated nanorods which were treated with $Pt(acac)_2$ for very short reaction times based on our previous report that this Pt-activation reaction occurs preferentially on the sulfur-rich nanorod terminus under kinetically controlled conditions.[3]

Control experiments: the role of reaction temperature during Co-deposition.

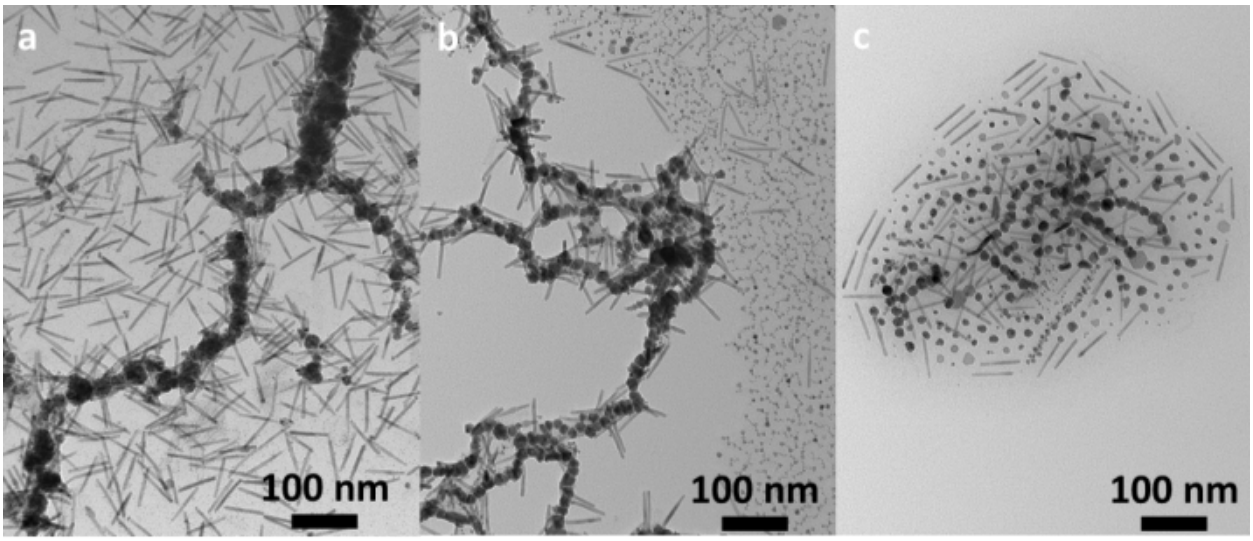

Figure S-6: TEM images of samples cast directly from the crude reaction mixture after Co-deposition onto Pt-activated nanorods at 120 °C for 15 minutes (a), 120 °C for 23 hours (b), and 200 °C for 15 minutes (c).

We also investigated the role of temperature during the Co-deposition reaction. The rate of decomposition of $Co_2(CO)_8$ increases with temperature, so controlling temperature is one way to control the feed rate of Co metal over time for a given concentration of $Co_2(CO)_8$. We observed that 160 °C was the optimal temperature for Co-deposition for the temperatures studied.

Co-deposition at lower temperature (120 °C versus 160 °C) resulted in few nanorods receiving a CoNP-tip, and a large polydispersity was observed in the CoNP-tips formed (Fig. S-6a). Allowing the reaction to proceed for longer times (120 °C, 23 hours versus 15 minutes) resulted in the formation of polydisperse free CoNPs along with an increase in the apparent number of tipped nanorods (Fig. S-6b). Co-deposition at higher temperature (200 °C versus 160 °C) resulted in the formation of free CoNPs with concomitant Co-deposition onto both termini of the Pt-activated nanorods, and CoNPs were also frequently observed to be present at lateral nanorod facets (Fig. S-6c). In general, the apparent number of CoNPs/nanorod increased with temperature over the range of temperatures studied (120 °C, 160 °C, and 200 °C).

Control experiment: modifying the Co-deposition conditions to yield dipolar CoNP-tips for nanorods activated for longer times.

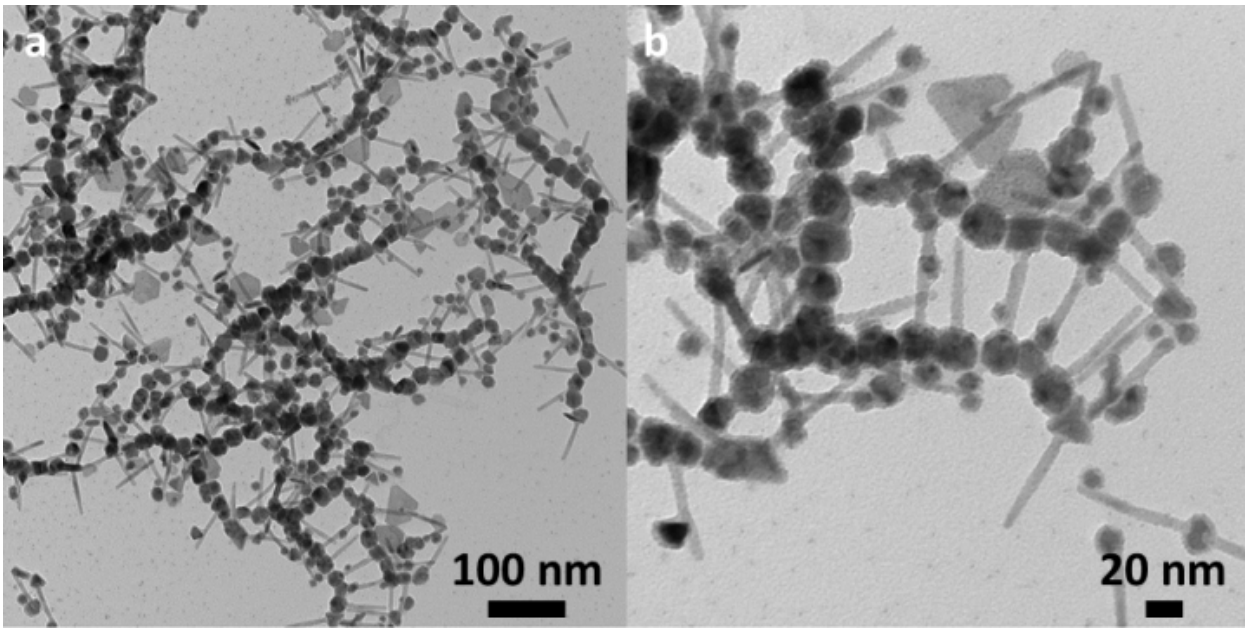

Figure S-7: Dipolar assemblies obtained from nanorods activated for 8 minutes (versus 30 seconds) by decreasing the concentration of Pt-activated nanorods used to 1/3 of that in the standard procedure (approximately 0.33 nmol Pt-activated nanorods). TEM images of samples cast directly from the crude reaction mixture after Co-deposition show that the dipolar assemblies formed contain a large fraction of dumbbell CoNP-tipped nanorods which provide branching points between neighboring chains (a) and form ladder-like structures (b).

As discussed in the manuscript, Co-deposition onto nanorods which were activated for longer times (or with higher concentrations of $Pt(acac)_2$) resulted in more CoNPs per nanorod, where the CoNP-tips were less frequently found to be dipolar as observed by their assembly. We then sought to increase the CoNP-tip diameter on these nanorods which were activated for longer times to ascertain whether the Co-deposition conditions could be modified to allow these intermediates could be used as precursors to dipolar CoNP-tipped nanorods.

A Co-deposition reaction was carried out using the same nanorods which were activated for 8 minutes shown in manuscript Fig. 1c, but using 1/3 the original concentration of Pt-activated nanorods (all other parameters were unchanged, Fig. S-7). The heterostructures formed using these nanorods activated for longer times again had CoNPs positioned frequently at both nanorod termini and along the lateral facets, though many of these CoNP-tips were now large enough to form dipolar assemblies. However, the resulting assemblies were highly branched structures. This branching was most evident in the formation of ladder-like structures, where two chains of CoNP-tips were oriented parallel to one another and bridged by CdSe@CdS nanorod linkers (Fig. S-7b).

4. Optical spectroscopy of Pt-activated nanorods

Optical spectroscopy of a representative sample of CdSe@CdS nanorods (nanorod length = 69.0 nm ± 6.5 nm, nanorod diameter = 5.9 nm ± 0.6 nm) was comparable before and after activation with $Pt(acac)_2$. UV-vis spectroscopy of nanorods at similar concentrations were taken in toluene before and after activation, and both samples showed similar absorbance profiles over the spectral window observed (Fig. S-8). Fluorescence quenching was not observed as demonstrated by the nearly identical emission spectra for native nanorods and Pt-activated nanorods at comparable optical density (Fig. S-9).

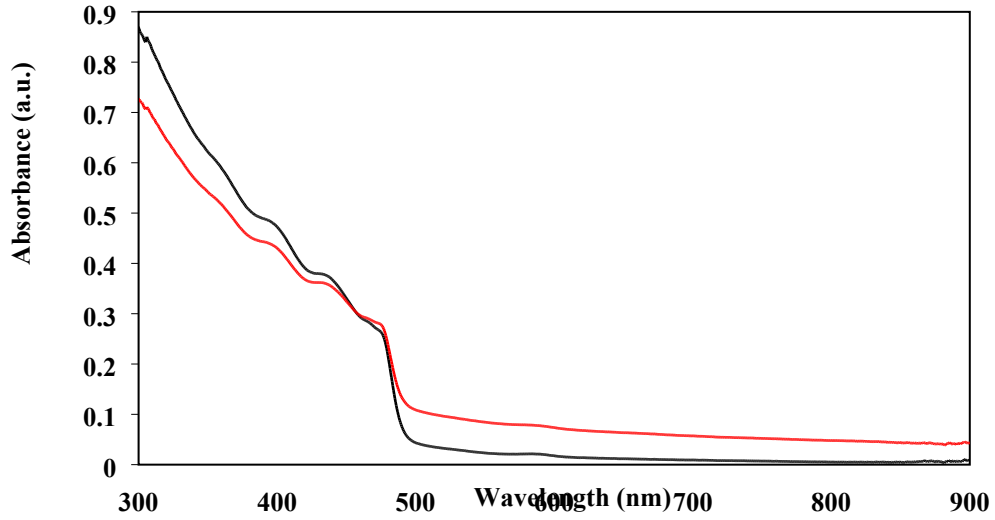

Figure S-8: UV-vis spectra for native CdSe@CdS nanorods (black line) and Pt-activated nanorods after 30 seconds reaction time (red line) at similar concentration. The UV-vis spectra were not scaled in any way for this figure. Nanorod dimensions: length = 69.0 nm ± 6.5 nm, diameter = 5.9 nm ± 0.6 nm.

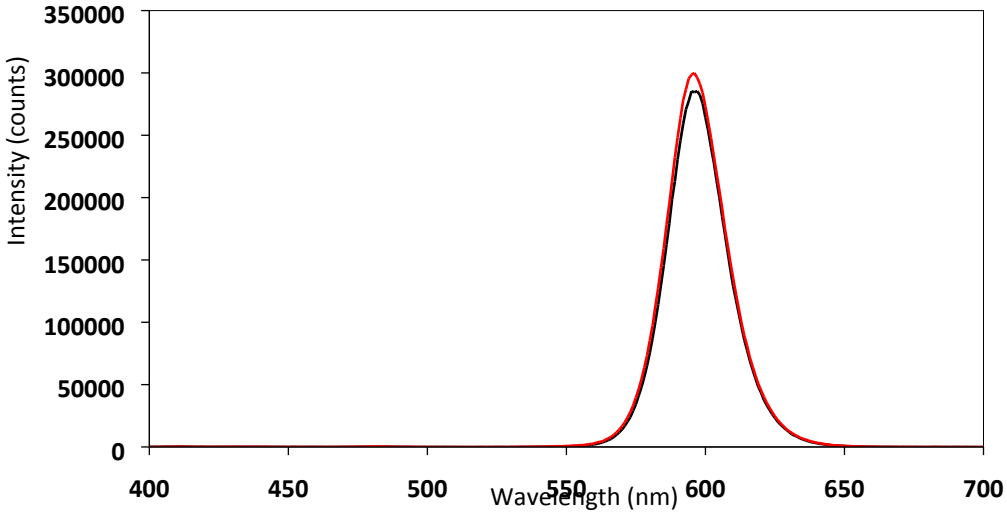

Figure S-9: Photoluminescence data for native CdSe@CdS nanorods (black line) and Pt-activated nanorods after 30 seconds reaction time (red line) at similar concentration. The fluorescence spectra were not scaled in any way for this figure. The excitation wavelength was 366 nm. Nanorod dimensions: length = 69.0 nm ± 6.5 nm, diameter = 5.9 nm ± 0.6 nm.

5. Higher resolution insets located in lower resolution TEM images (from Fig. 3 in the manuscript)

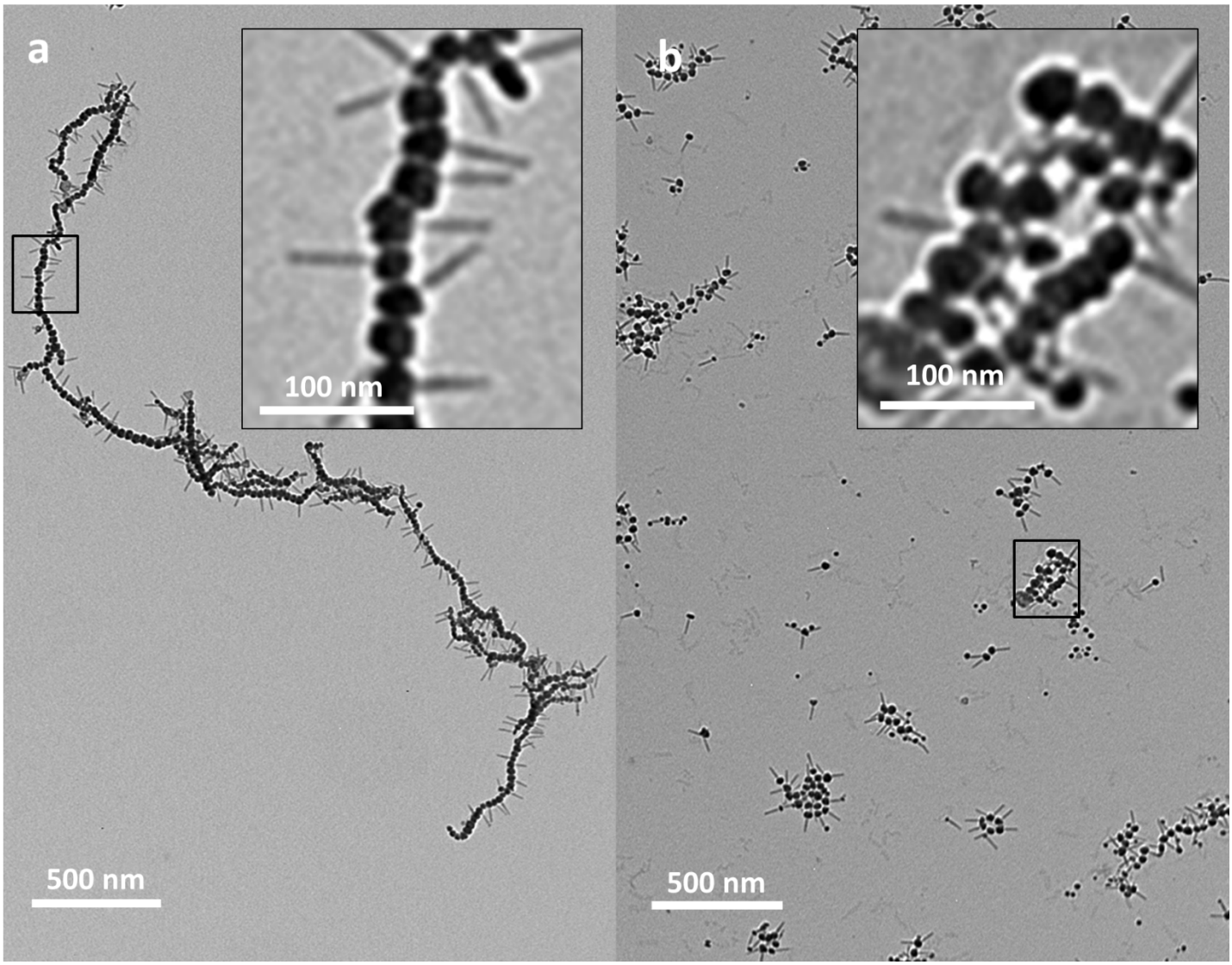

Figure S-10: (a) Low resolution TEM image of dipolar CoNP-tipped matchstick nanorods prepared from optimized Pt-activated nanorods (from Fig. 1b, L = 64.1 + 5.4 nm; D = 5.7 + 0.6 nm,), with higher resolution inset taken from the region described by the black rectangle ($D_{CoNP\text{-}tip}$ = 22.4 $\pm$ 4.7 nm). (b) Low resolution TEM image of dipolar matchstick and dumbbell CoNP-tipped nanorod mixtures prepared from PtNP-tipped nanorods obtained from longer Pt-activation times (from Fig. 1c), with higher resolution inset taken from the region described by the black rectangle ($D_{CoNP\text{-}tip}$ = 23.0 $\pm$ 4.8 nm).

Fig. S-10 is included to enable direct comparison of the higher resolution insets with lower resolution images for the samples shown in manuscript Fig. 3. The TEM image shown in Fig. 3a,b of the manuscript contain higher resolution insets of the same *samples* taken from slightly different regions of the *TEM grids* (Fig. 3a).

References:

1. W. W. Yu, L. H. Qu, W. Z. Guo and X. G. Peng, *Chem. Mater.*, 2003, **15**, 2854-2860.
2. O. Paris, C. Li, S. Siegel, G. Weseloh, F. Emmerling, H. Riesemeier, A. Erko and P. Fratzl, *J. Appl. Crystallogr.*, 2007, **40**, s466-s470.
3. L. J. Hill, M. M. Bull, Y. Sung, A. G. Simmonds, P. T. Dirlam, N. E. Richey, S. E. DeRosa, I.-B. Shim, D. Guin, P. J. Costanzo, N. Pinna, M.-G. Willinger, W. Vogel, K. Char and J. Pyun, *ACS Nano*, 2012, **6**, 8632-8645.

4. L. Carbone, C. Nobile, M. De Giorgi, F. D. Sala, G. Morello, P. Pompa, M. Hytch, E. Snoeck, A. Fiore, I. R. Franchini, M. Nadasan, A. F. Silvestre, L. Chiodo, S. Kudera, R. Cingolani, R. Krahne and L. Manna, *Nano Lett.*, 2007, **7**, 2942-2950.
5. S. E. Habas, P. D. Yang and T. Mokari, *J. Am. Chem. Soc.*, 2008, **130**, 3294-3295.
6. B. D. Korth, P. Keng, I. Shim, S. E. Bowles, C. Tang, T. Kowalewski, K. W. Nebesny and J. Pyun, *J. Am. Chem. Soc.*, 2006, **128**, 6562-6563.
7. P. Y. Keng, I. Shim, B. D. Korth, J. F. Douglas and J. Pyun, *ACS Nano*, 2007, **1**, 279-292.
8. M. M. Bull, W. J. Chung, S. R. Anderson, S.-j. Kim, I.-B. Shim, H.-j. Paik and J. Pyun, *J. Mater. Chem.*, 2010, **20**, 6023-6025.
9. S. Deka, A. Falqui, G. Bertoni, C. Sangregorio, G. Poneti, G. Morello, M. De Giorgi, C. Giannini, R. Cingolani, L. Manna and P. D. Cozzoli, *J. Am. Chem. Soc.*, 2009, **131**, 12817-12828.